Eur. Phys. J. D **30**, 37–47 (2004)
DOI: 10.1140/epjd/e2004-00053-y

THE EUROPEAN PHYSICAL JOURNAL D

The threshold electron impact spectrum of molecular oxygen

J.J. Jureta[a] and S. Cvejanovic

Institute of Physics, Pregrevica 118, P.O. Box 68, 11080 Zemun, Serbia and Montenegro

Received 13 October 2003 / Received in final form 13 January 2004
Published online 20 April 2004 –

Abstract. The threshold electron impact spectrum of molecular oxygen has been studied using a high energy resolution electron spectrometer in the energy region 2–15.2 eV and the penetrating field method for scattered electrons. The measured features such as core excited resonances as well as Rydberg and valence states are measured in threshold and metastable spectra. They are identified and assigned according to their energy positions, energy spacing between vibrational levels and compared with similar data from the literature. A good agreement was found in the energy positions between measured features and corresponding potential energy diagram for Rydberg states for molecular oxygen given by Morrill et al. [1].

PACS. 34.80.Gs Molecular excitation and ionization by electron impact

1 Introduction

Due to its great importance, molecular oxygen has been studied very extensively in the past both theoretically and experimentally. The great effort from both sides was done in order to explain the very complicated picture seen in the energy region of the Schumann-Runge continuum from 8 to 10 eV of the incident electron energy. Unfortunately, there are still disagreements between theoretical calculations and experimental results concerning this energy region. Experimental techniques used to study the excited states of O_2 arise from three groups: the first group is optical spectroscopy which uses a laser beam such as resonance-enhanced multiphoton ionisation (REMPI) and single-photon absorption (SPA). The second group is translational spectroscopy (KER analysis) and the third group that uses an electron beam is the energy-loss spectroscopy (EEL). Theoretical treatments are based on ab initio and coupled-channel Schrödinger equation calculations (CSE).

Another technique which uses an electron beam is threshold spectroscopy, and until now it hasn't been used for studying the excitation of molecular oxygen. This technique allows to detect those scattered electrons which have very low energy ($\leq$20 meV), which gives the opportunity to detect those excited states not seen in the energy loss technique at high impact energy due to the selection rules. The threshold technique combined with high energy resolution in the incident electron beam allows detection not only of electronic states such as valence and Rydberg states but the negative ions (resonances) too. Hence, the measured signal in the threshold spectra represents contributions from non resonant and resonant scattering.

[a] e-mail: jureta@fyam.ucl.ac.be

A critical review of the work done on molecular oxygen prior to 1972 was published by Krupenie [2]. The recent papers from optical [3] and electron impact studies [4] indicate that research on the excitation of molecular oxygen is still of interest.

In this paper, we present the results of electron impact excitation of O_2 using threshold spectroscopy which includes the high resolution electron spectrometer in the incident electron beam and the penetrating field method for scattered electrons. In that way we were able to detect a signal that comes from optically forbidden transitions and resonances.

2 Experimental procedure

The experimental set-up used to study the excitation process of O_2 ($e + O_2 \rightarrow O_2^* + e$) is a crossed beam electron spectrometer. It consists of the three components, a monochromator with an electron gun and lenses, the target region and analyser with accompanying lens and detector. Electrons are produced in a Pierce type electron gun by thermionic emission. The electron beam with a well defined geometry before the hemispherical monochromator is formed by a system of a three-element aperture lenses. Between the monochromator and the interaction region, the electron beam passes two sets of lenses made of three and four electrodes with apertures in order to satisfy the constant focusing in the incident energy range from 0.1 to 100 eV (see Cvejanovic et al. [5]). So formed, the electron beam with an energy spread of typically 30 meV (FWHM) and intensity of 1–2 nA is focused in the middle of the interaction region where it crosses a gas beam effusing from a gold-plated platinum-iridium tube 2 mm

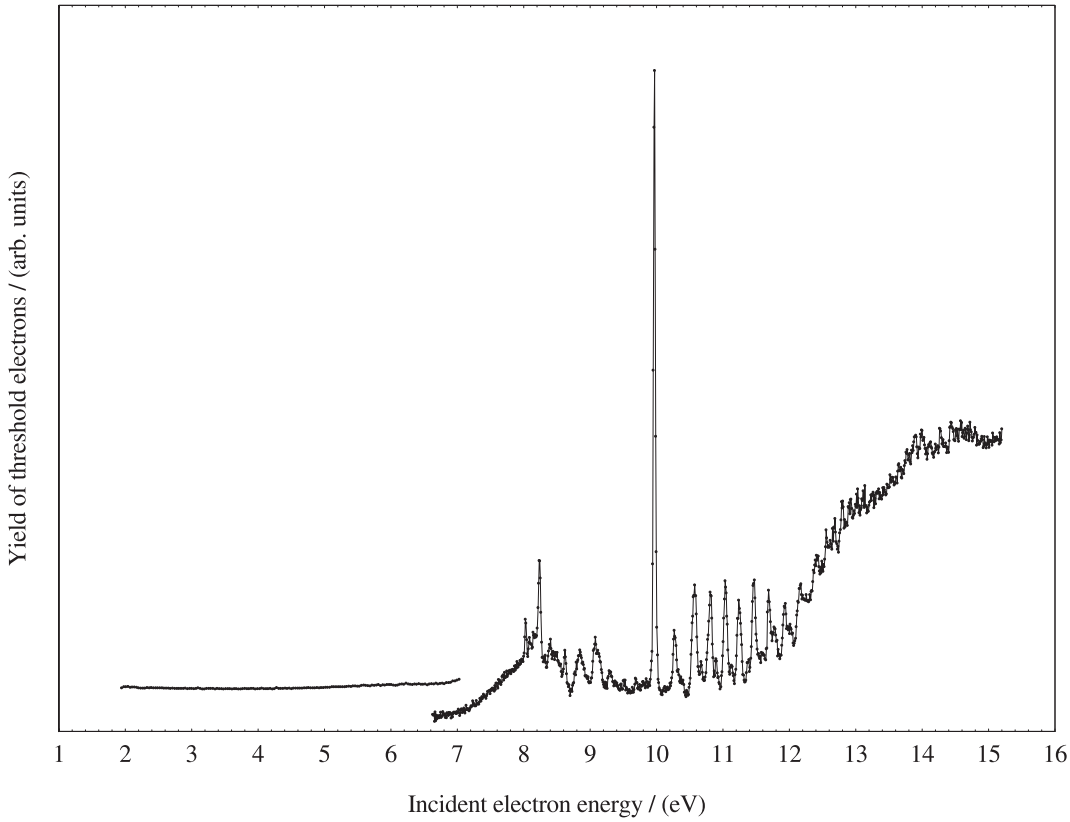

Fig. 1. Threshold electron impact spectrum of O_2 in the energy region 2–15.2 eV.

away from the incident beam. The target region is surrounded by a cylinder made from a mesh of transparency of 80% with four apertures, two for the incident electron beam, one for a gas needle and a side opening toward the extraction electrode. A positive potential difference from 0 to 15 V between the extractor and the surrounding mesh produces a nonuniform electric field inside the interaction region and a saddle point in the equipotential surface at the interaction region where the electron beam crosses the molecular beam. Scattered electrons with an energy distribution between zero and several ($\leq$10) meV are trapped by this potential distribution and tunnelled toward a small mirror analyser. This technique is based on the principle of the well-known field penetration method described in detail by Cvejanovic and Read [6], and further improved by Cvejanovic et al. [7]. The electrostatic analyser is a double pass cylindrical mirror analyser preceded by a three-cylinder electrostatic lens and with a detector (channeltron) mounted directly to an exit of the analyser. This detection system enables us to detect scattered electrons of different energies with a good control of the transmission in the scattered electron range from 0.2 to 2 eV.

The detector for metastable states is positioned opposite the gas tube at a distance of 20 mm from the electron beam and allows the determination of the energy location of the negative ion (resonance) states.

The spectrometer operates in four different modes: constant residual energy mode (CRE), energy loss mode (EL), threshold electron spectroscopy mode (TES) and excitation function mode (EF). In the TES mode the detection part is optimised to detect scattered electrons with near zero energy during the sweeping of the incident electron energy. In this mode it is possible to detect scattered electrons with energy between zero and 20 meV, though we mainly detected electrons of 10 meV energy which was easy to verify from the measured ratios $2^1S/2^3S$ in threshold spectra of helium [6].

3 Results and discussion

The threshold spectrum of O_2 in the energy region from 2 to 15.2 eV is shown in Figure 1. The spectrum is composed of two parts collected over different intervals of time. The first part between 2 and 7 eV has better statistics and is shown separately from the second part in the same figure. The best energy resolution in the spectrum was 28 meV. Detailed spectra in the energy region 6.6–10 eV and 10–15.2 eV with assignments of the features are shown in Figures 2 and 4 respectively. The classification of the observed features is given in Tables 1–5. The energy scale was calibrated in two different ways: with respect to the spectroscopic energy position of the longest band at 9.970 eV, the most intense structure in the threshold spectrum and from the mixture of molecular oxygen with xenon. The uncertainty in the energy scale is not higher than 10 meV.

Table 1. Excitation energies (eV) of the $^3\Pi_g(R)$ Rydberg state from the threshold spectra. Comparison with other measurements.

State $^3\Pi_g(R)$		Present results	E (eV) [19]	E (eV) [21]	E (eV) [20]	E (eV) [22]	E (eV) [1]	E (eV) [24]	E (eV) [25]
$\nu' =$	0	8.151	8.145	8.138	8.15	8.144	8.140	8.148	8.838
	1	8.401	8.366	8.372	8.36	8.383	8.379	8.378	9.065
	2	8.619	8.610	8.614	8.60	8.611	8.611	8.603	9.287
	3	8.838	8.835	8.840	8.83	8.840	8.837	8.833	9.507
	4	9.068	-	-	-	-	9.054	9.048	-
	5	9.302	-	-	-	-	9.273	9.283	-
	6	9.510	-	-	-	-	9.488	9.503	-
	7	-	-	-	-	-	9.697	9.713	-
	8	-	-	-	-	-	9.900	9.925	-

Table 2. Excitation energies (eV) of the $^1\Pi_g(R)$ Rydberg state from the threshold spectra. Comparison with other measurements.

State $^1\Pi_g(R)$		Present results	E (eV) [20]	E (eV) [23]	E (eV) [1]	E (eV) [24]	E (eV) [22]	E (eV) [25]
$\nu' =$	0	8.234	8.60	8.228	8.228	8.218	8.232	8.837
	1	8.458	8.83	8.46	8.460	8.443	8.464	9.055
	2	8.698	9.05	8.70	8.681	8.689	8.686	9.270
	3	8.932	9.27	8.92	8.921	8.915	-	9.482
	4	9.140	-	-	9.144	-	-	-
	5	9.380	-	-	9.360	9.385	-	-
	6	-	-	-	9.572	9.590	-	-
	7	-	-	-	9.786	9.810	-	-
	8	-	-	-	9.994	10.010	-	-

Table 3. Excitation energies (eV) of the observed resonances in the present experiment. Comparison with the measurements of Sanche and Schulz [10].

Present results		[10]	
E (eV)	Label	E (eV)	Label
8.02	**A**	8.03–8.06	1-1′
8.10	**B**	8.12	2
8.23	**C**	8.23–8.26	3-3′
8.47	**D**	8.48–8.54	5-5′
8.94	**E**	8.90–8.98	7-7′
9.13	**F**	-	-
9.39	**G**	9.36–9.44	10-10′
9.68	**H**	-	-
9.97	**I**	9.86–9.92–9.98	13-13′-13″
		10.43–10.48	14-14′
10.53	**J**	10.53–10.61	15-15′
10.74	**K**	10.74–10.82	16-16′
10.92	**L**	10.91–11.00	17-17′
		Band "**a**"	
11.73		11.81	$\nu = 1$
11.90		11.95	$\nu = 2$
12.08		12.07	$\nu = 3$
12.32		12.19	$\nu = 4$
12.56		12.31	$\nu = 5$
12.77		12.42	$\nu = 6$
12.88		12.53	$\nu = 7$
12.98		12.64	$\nu = 8$
13.08		12.75	$\nu = 9$
13.18		12.86	$\nu = 10$

3.1 Energy region 2–7 eV

The first part of the threshold spectrum from 2 to 7 eV with better statistics is shown in Figure 1 in the form of a smooth curve without any internal structure. Above 2 eV, the threshold spectrum does not show any contributions from high vibrational levels of the $b^1\Sigma_g^+$ state seen in energy loss spectra [4]. The first broad and weak maximum situated between 5 and 7 eV cannot be undoubtedly identified. The detailed theoretical calculations [1] show three potential curves traversing the F-C region very close to each other, $A^3\Sigma_u^+$, $A'^3\Delta_u$ and $C^1\Sigma_u^-$, that belong to the optically allowed transitions (g-u). So, the weak signal in the threshold spectra from 5 to 7 eV probably originates from these three states, which belong to the optically allowed transitions and hence cannot be strong in the threshold spectra where the optically forbidden transitions are dominant.

This part of the threshold spectra can only be compared with the energy loss spectra of O_2 [4] taken at a residual energy of 2 eV and scattering angle of 90°. The difference is quite obvious, the energy loss spectrum shows high vibrational levels of the $b^1\Sigma_g^+$ state and a strong maximum between 5 and 7 eV not seen in threshold spectra indicating that this part of the threshold spectra is not influenced by $O_2^{-2}\Pi_g$ shape resonance responsible for the electronic excitation of the first two electronic states $a^1\Delta_g$ and $b^1\Sigma_g^+$ recorded at higher residual energy in the energy-loss spectra. Theoretically, the resonant effect was studied by [8,9]. Both calculations confirmed the existence of the $O_2^{-2}\Pi_g$ shape resonance which decays into three channels as parents $O_2(X^3\Sigma_g^-)$, $O_2(a^1\Delta_g)$

Table 4. Excitation energies (eV) of the observed structures in the threshold spectrum in the energy region 9.9–12.2 eV. Comparison with the measurements of York and Comer [22] and Yokelson et al. [35].

Present result		[22]		[35]	
	E (eV)	E (eV)	Label	E (eV)	
State $E^3\Sigma_u^-$					
$\nu' = 0$	9.970	9.970	LB		
1	10.273	10.288	SB		
2	10.570	10.576	TB		
State $4^{1,3}\Pi_g(R)$				$4^3\Pi_g(R)$	$4^1\Pi_g(R)$
$\nu' = 0$	10.367			10.337	10.360
1	10.570			10.571	10.592
2	10.812	10.804	6	10.799	10.820
3	11.031	11.035	10	11.023	11.044
4	11.242	11.240	18	11.240	
5	11.469	11.467	18		
6	11.687	11.707	18		
7	11.930	11.926	18		
8	12.156	12.157	18		
State $^3\Pi_u$					
$\nu' = 0$	10.672	10.664	4		
1	10.898	10.912	7		
2	11.133	11.123	11		
3	11.383	11.378	13		
4	11.593	11.554	15		
5	11.781	11.779	17		
6	12.008	12.007	19		

and $O_2(b^1\Sigma_g^+)$. A multichannel effective range theory [9] was used in order to calculate the cross-section for this resonance. They found that the cross-section curve starts at 1 eV and has a broad maximum between 4 and 10 eV. Experimentally, this was confirmed by [4], where the absolute differential cross-sections for the excitation of $a^1\Delta_g$ and $b^1\Sigma_g^+$ states were measured.

3.2 Resonant scattering in the energy region 8–10 eV

The resonant contribution to the threshold spectra in the energy region between 8 and 10 eV is manifested in three different forms: as narrow isolated structures, as shoulders above the corresponding vibrational levels and as the structure the excitation energy which coincides with the threshold energy of corresponding vibrational level. Molecular oxygen is one of the examples where core excited resonances dominate in the energy region very close to the threshold energies of the excited states. These features can only be detected in those experiments at very low residual energy as for example the energy-loss experiments at low impact electron energy and low residual energy and in threshold spectroscopy. The first experimental evidence of core excited resonances in O_2 were published by Sanche and Schulz [10] by using high resolution transmission spectroscopy. In the energy region between 8 and 10 eV they detected 13 resonances forming an irregular progression. Two of them (see Tab. 3) labelled (1-1′) and (3-3′) are very narrow features with estimated natural

Table 5. Excitation energies (eV) of the observed structures in the threshold spectrum in the energy region 12.2–15.2 eV. Comparison with the measurements of York and Comer [22] and Sanche and Schulz [10].

Present results		[22]		[10]	
E (eV)	Label	E (eV)	Label	E (eV)	
				band "**a**"	
12.406	**J1**	12.414	**i**	12.42	$\nu = 6$
12.547	**J1**	12.546	**i**	12.53	$\nu = 7$
12.672	**J1**	12.669	**i**	12.64	$\nu = 8$
12.789	**J1**	12.786	**i**	12.75	$\nu = 9$
				12.86	$\nu = 10$
12.906	**J2**	12.908	**ii**		
13.023	**J2**	13.018	**ii**		
13.117	**J2**	13.120	**ii**		
13.531	**M'**	13.517	**M'**		
13.641	**M'**	13.625	**M'**		
13.758	**M'**	13.724	**M'**		
13.883	**J**	13.863	**J**		
13.992	**J**	13.990	**J**		
14.117	**J**	14.116	**J**		
				Band "**b**"	
14.273	**J3**	14.278	**iii**	14.29	
14.430	**J3**	14.430	**iii**	14.45	
14.570	**J3**	14.564	**iii**	14.60	
14.711	**J3**	14.716	**iii**	14.74	

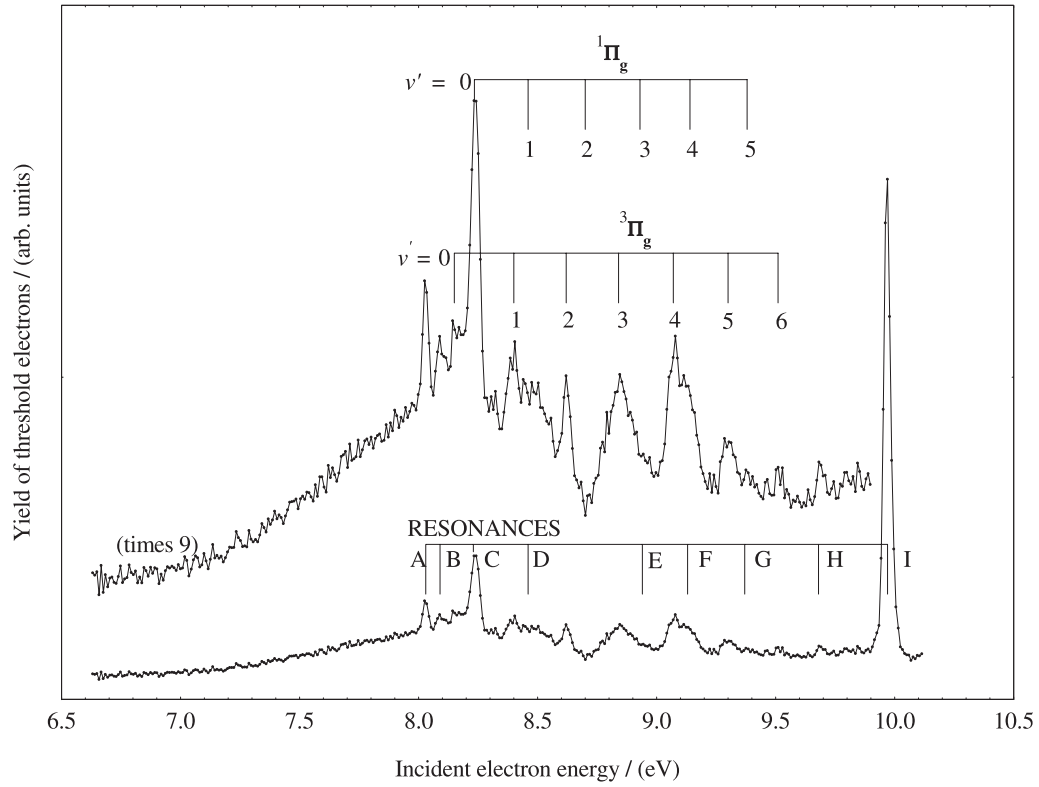

Fig. 2. Part of the threshold spectra from Figure 1 in the energy region 6.6–10 eV. The spectrum shows Rydberg states and resonances.

widths of less than 10 meV. The spacing of 210 meV between them was one of the arguments for the conclusion that resonances consist of two Rydberg electrons bound to a $X^2\Pi_g$ ionic core with $^3\Pi$ and $^1\Pi$ Rydberg states as parent states. Other resonances have different widths and do not form a regular progression which was explained by the predissociation of the O_2^- vibrational progression above the first vibrational level. The second evidence for the existence of core excited resonances in O_2 is seen in threshold spectra of O_2 shown in Figure 2. The spectrum shows 9 resonances (**A**-**I**) (Tab. 3) identified according to their energy positions and their behaviour in spectra with different residual energies [11]. In that way, two very narrow structures at 8.02 and 8.10 eV are identified as two members of the vibrational progressions of the O_2^- resonances. The third member of this progression at 8.23 eV coincides in energy with $\nu' = 0$ of the $^1\Pi_g$ Rydberg state and is responsible for its enhancement. The first feature **A** at 8.02 eV is a very narrow structure whose width is limited by the resolution of the spectrometer. The measured FWHM of 28 meV corresponds to a lifetime of 2×10^{-14} s which is comparable with the vibrational period of the O_2 molecule. However, the natural width of this feature must be less than 10 meV and correspond to a lifetime of 10^{-13} s giving the possibility of forming the vibrational progressions manifested in the spectra. The energy positions of resonances **A**, **B** and **C** are in quite good agreement with the resonances (1-1′), 2 and (3-3′) [10], considering their minimum energy positions (derivative of the transmitted signal). All three resonances are situated above the $^3\Pi_g$ valence state and only the first resonance **A** has no influence on the $^3\Pi_g$ Rydberg state. Two other resonances are not well defined due to a perturbation by the nearest vibrational levels of the Rydberg electronic states. In that way, the threshold spectra confirmed the existence of the core excited resonances in the O_2 molecule and supported the idea of Sanche and Schulz [10] about their perturbation above the first vibrational level of O_2^-.

Resonant contributions in the form of shoulders above the nearest vibrational levels of the Rydberg states in threshold spectra (Fig. 2) are visible at energies 8.47 (**D**), 8.94 (**E**), 9.13 (**F**) and 9.39 (**G**) eV (Tab. 3). They are situated above the $\nu' = 1$, 3, 4 and 5 vibrational levels of the $^3\Pi_g$ Rydberg states respectively causing their broadening. The energy positions of these four resonances are in quite good agreement with the resonances (5-5′), (7-7′), and (10-10′) in the transmission experiment [10]. On the other hand, the threshold spectra do not give any evidence for the existence of a resonance which coincides with energy of the resonance (9-9′) (9.16−9.23) eV found by Spence [12], who concluded that only this resonance decays into the $^3\Pi_g$ Rydberg state.

The last two resonances present in the form of isolated sharp features in the threshold spectra below 10 eV are **H** and **I** at 9.68 and 9.97 eV. The resonance **H** does not coincide with the energy of any vibrational level of Rydberg states, while resonance **I** coincides with energy of $\nu' = 0$ of the $E^3\Sigma_u^-$ state historically known as the longest band and is responsible for its strong enhancement [13].

The energy position of the resonance **I** is in good agreement with the resonance (13-13′-13″) [10].

3.3 Non-resonant scattering in the energy region 7–10 eV-valence states

The valence states of the O_2 molecule in the threshold spectra (Fig. 2) in the energy region 7–10 eV are presented in the form of maxima which lie below the structures identified as Rydberg states and resonances. The broad feature between 7 and 9 eV (see Fig. 2), with a maximum at 8.2 eV can be identified according to the potential energy curve diagram [1]. Inside the F-C region the potential energy diagram shows $II^3\Pi_g$, $B^3\Sigma_u^-$, $^1\Pi_g$ and $^{1,3}\Pi_g$ states. Considering the very good agreement in energy position of this maximum in the threshold spectra with the energy position of the $II^3\Pi_g$ valence state [1] in the F-C region, we concluded that this maximum arises from the $II^3\Pi_g$ valence state but not from the optically allowed $B^3\Sigma_u^-$ state. Also, this is in very good agreement with the results of Cartwright et al. [14], who found that the $^3\Pi_g$ valence state contributes significantly to a continuum in the energy range of 7 to 8.2 eV from a decomposition of the photo absorption spectrum of the Schumann-Runge continuum of O_2. Contrary to these results, Spence [12] found that the $^3\Pi_g$ valence state traverses the F-C region between 7.6 and 7.8 eV in measurements of the ejected electron energies resulting from the decay of O_2^- states. In the photo dissociation experiment of O_2 Lee et al. [15] concluded that the $^3\Pi_g$ and $^3\Pi_u$ valence states do not contribute significantly to the continuum in the energy region 7–10.69 eV. This last conclusion is in accordance with the theoretical results of Buenker et al. [16], Julienne et al. [17] and Saxon and Liu [18].

The second weak maximum in the threshold spectra from 8.7 to 9.6 eV is not well defined, it has a lower intensity than the former maximum and is covered by two broad structures. The energy position of this maximum corresponds well to the energy position of the $II^1\Pi_g$ valence state from an energy diagram of the potential energy curves of O_2 [1].

3.4 Rydberg states in the energy region above 8 eV

The threshold spectrum in Figure 2 shows several features above 8 eV identified as $3s\sigma_g\,^{1,3}\Pi_g$ Rydberg states according to their energy positions and a regular spacing between vibrational levels. The features occupy the energy region known as the Schumann-Runge continuum. In the spectra they have different intensities and widths superimposed on the underlying continuum, which comes from the valence states. Rydberg states were discovered in the past by energy loss experiments, REMPI, PES and translational spectroscopy. Their existence was confirmed by theoretical calculations too. The agreement between theory and experiment is not quite satisfactory. The identification of singlet and triplet Rydberg states in the threshold spectra is done by using potential energy curves of O_2 [1].

The $^3\Pi_g$ Rydberg state was observed earlier in energy loss measurements [19–22]. Four vibrational levels were detected in each of these experiments. Sur et al. [23] observed 5 vibrational levels, while van der Zande et al. [24] obtained 9 vibrational levels using translational spectroscopy. Table 1 shows the energy positions of the vibrational levels of the $^3\Pi_g$ Rydberg state from the present measurement together with the results of other authors. It is clear that the energy positions of the first four vibrational levels are in good agreement between the threshold and other measurements except the result from a theoretical calculation [25]. The threshold spectrum from Figure 2 clearly shows that the $\nu' = 0$ level is very low in intensity due to the weak coupling between this state and the ground state of O_2 in the F-C region, which is seen from the energy diagram of the potential energy curves of O_2 [1]. This weak coupling is the consequence of different equilibrium nuclear positions between the Rydberg and ground state of molecular oxygen. The second reason for its low intensity arises from the $^3\Pi_g$ valence state which shows the maximum intensity in this part of the spectra indicating the predissociation of this level. This is in accordance with the prediction of [1,23] that the crossing point between the Rydberg and valence states is at the bottom of the $^3\Pi_g$ Rydberg potential well. The $\nu' = 1$ of the $^3\Pi_g$ Rydberg state is shown in the threshold spectra with low intensity due to the predissociation by the $^3\Pi_g$ valence state. This level is not separated from the corresponding level of $\nu' = 1$ of the $^1\Pi_g$ Rydberg state probably due to the influence of the resonance **D** (Fig. 2). The $\nu' = 2$ level of the $^3\Pi_g$ Rydberg state is not influenced by any resonant contribution. This level is also partly influenced by the predissociation of the $^3\Pi_g$ valence state but it has the form of a narrow isolated peak. Using REMPI spectroscopy Sur et al. [23] have found that only this level shows rotationally resolved structure, while the other vibrational levels are all diffuse. Levels $\nu' = 3$ and 4 are more intense and broad due to an influence of resonances **E** and **F** which are situated above these levels respectively. These levels are not separated by the nearest $^1\Pi_g$ Rydberg states and their intensities indicate that the predissociation of $^3\Pi_g$ and $^1\Pi_g$ valence states is relatively weak. The last two levels $\nu' = 5$ and 6 are not influenced by the resonance but their intensities indicate their predissociation of the $^1\Pi_g$ valence state too.

The $^1\Pi_g$ Rydberg state was identified earlier in energy loss experiments [20,22], in a multiphoton ionisation experiment [23] and in translational spectroscopy [24]. Their results together with our measurements are shown in Table 2. The table shows excellent agreement in the energy positions of the first two vibrational levels between the present measurement and [22–24], but not with the measurement in [20] and the theoretical calculations in [25]. In the present measurement we identify only 5 vibrational levels ($\nu' = 0$, 1, 3, 4 and 5) of the $^1\Pi_g$ Rydberg state. Except for the $\nu' = 0$ level the other peaks are not precisely identified due to the perturbation by the $^3\Pi_g$ and $^1\Pi_g$ valence states. The $\nu' = 0$ level is present as an enhanced peak, second in intensity in the threshold spectra,

and whose intensity is the consequence of the resonant contribution (resonance **C** in the spectra). The resonance has an excitation energy equal to the threshold energy of this level giving its strong enhancement. Without any resonant contribution the $\nu' = 0$ level should be present as a peak of small intensity due to the weak coupling between this state and the ground state of the molecular oxygen which is the consequence of different equilibrium positions between the ground and Rydberg state in the F-C region (see the potential energy diagram by Morrill et al. [1]). One can conclude that the main contributions to the intensity of this level arise from the resonant contribution. The spectra do not give clear evidence for its predissociation of the spin-orbit interaction with $\nu' = 0$ of the $^3\Pi_g$ Rydberg state as was seen in translational spectroscopy [24]. The $\nu' = 1$ level of the $^1\Pi_g$ Rydberg state is present in the threshold spectra in the form of a very broad feature with low intensity indicating that it is strongly perturbed by the nearest $^3\Pi_g$ valence state. Hence its energy position is not precisely defined. From the threshold spectra the influence of the resonance **D** on the intensity of this level is not clear. The $\nu' = 2$ level is present in the spectra in a form of a dip with a minimum energy of 8.70 eV indicating a complete predissociation of the $^1\Pi_g$ valence state. In that way the energy position of the $^1\Pi_g$ valence state is precisely defined in the F-C region. The crossing point between the $^1\Pi_g$ Rydberg and the $^1\Pi_g$ valence state is at 8.70 eV of the potential energy, which is little bit higher in energy than the crossing point in the diagram [1]. It is interesting to note that resonance **E** in the threshold spectra has no significant contribution in this energy region. The $\nu' = 2$ level is one of the examples of the Rydberg-valence mixing carefully examined by [24,26]. In the REMPI spectroscopy [26] the $\nu' = 2$ level appears as two distinct features. In their calculation they found that the feature is 64% Rydberg in character at lower energy, and 66% valence in character on the higher energy side. In the threshold spectra the $\nu' = 3$ and 4 levels of $^1\Pi_g(R)$ are not separated from the $\nu' = 3$ and 4 slevels of the $^3\Pi_g$ Rydberg state. This broadening is not a consequence of a lack in the spectrometer resolution but it arises from the perturbation of the $^1\Pi_g$ valence state and resonant contributions from **E** and **F** resonances. According to the present measurements it is not possible to conclude which contribution is dominant. Hence, the energy positions of these two levels are not precisely determined. The $\nu' = 5$ level appears at very low intensity due to the predissociation of the $^1\Pi_g$ valence state. The very low intensity of this level indicates the absence of any contribution from resonance **G** in the spectra.

3.5 Rydberg-valence mixing

The existence of Rydberg and valence states of the same symmetry in the energy region of 7 to 10 eV makes this region very complex. The interaction between the Rydberg and valence states has been the subject of many theoretical calculations and experimental verifications. Unfortunately, there is no mutual agreement concerning the intensity of the interaction. Buenker et al. [16], Saxon and Liu [25] concluded that for $^3\Pi_g$ states only the weak interaction between the Rydberg and valence states exists. Both calculations predict that the valence state crosses the Rydberg state between the first two vibrational levels. Li et al. [27] found a weak interaction of about 700–800 cm^{-1} between $n = 3$ Rydberg-valence states. Sur et al. [23] have concluded that the interaction between the $^3\Pi_g$ Rydberg and valence states is expected to be weak. The CSE calculations [1] show that the perturbation and predissociation in the singlet and triplet Rydberg states arise principally through Rydberg-valence interactions. On the other hand, energy-loss experiments do not give any quantitative information about the Rydberg-valence interaction. Spence [12] found that the interaction between the Rydberg and valence $^3\Pi_g$ states is much stronger resulting in the perturbation of the valence state such that it traverses the F-C region in the very narrow energy range between 7.6 and 7.8 eV.

From the threshold spectra one can conclude that the interaction between the Rydberg and valence states exists in the form of a deformation or broadening of the Rydberg states by the presence of valence states in the form of an underlying non-linear continuum. The spectra indicate that the $^3\Pi_g$ Rydberg state is predissociated by the $^3\Pi_g$ valence state between first two vibrational levels which is in agreement with the theoretical predictions [16,25]. The $^1\Pi_g$ Rydberg state is predissociated by the $^1\Pi_g$ valence state at an energy of 8.70 eV in the F-C region which agrees with the potential energy diagram of molecular oxygen [1].

3.6 Resonant scattering in the energy region 9.9–15.2 eV

In this energy region the resonances are obtained in two different ways, in the excitation function mode and metastable excitation function mode. The excitation energies of the measured features from both modes are summarized in Table 3 together with the results of Sanche and Schulz [10]. The resonant contribution to the threshold spectrum in Figure 4 in the energy region 9.9–11 eV is recognizable in the form of enhanced peaks at 9.970 eV and 10.570 eV. The resonance **I** [13] measured in the excitation function of the $^3\Pi_g(R)$ $\nu' = 1$ state at 90° and $\Delta E = 8.40$ eV is responsible for the intensity enhancement of the $E^3\Sigma_u^-$ $\nu' = 0$ state. Three other resonances measured in the excitation function of the $E^3\Sigma_u^-$ $\nu' = 0$ state at 90° and $\Delta E = 9.97$ eV have energies at 10.53, 10.74 and 10.92 eV respectively. The resonance **J** at 10.53 eV situated 40 meV below the $\nu' = 2$ $E^3\Sigma_u^-$ does not have as strong an influence on the intensity of this level as the resonance **I** at 9.97 eV. Similar behaviour is found for resonances **K** and **L** and their influence on the intensities of the nearest vibrational levels of the $n = 4$ Rydberg state. Table 3 shows a good agreement in the energy positions of the measured resonances **J**, **K** and **L** with resonances (15-15′), (16-16′) and (17-17′) respectively in the transmission experiment [10].

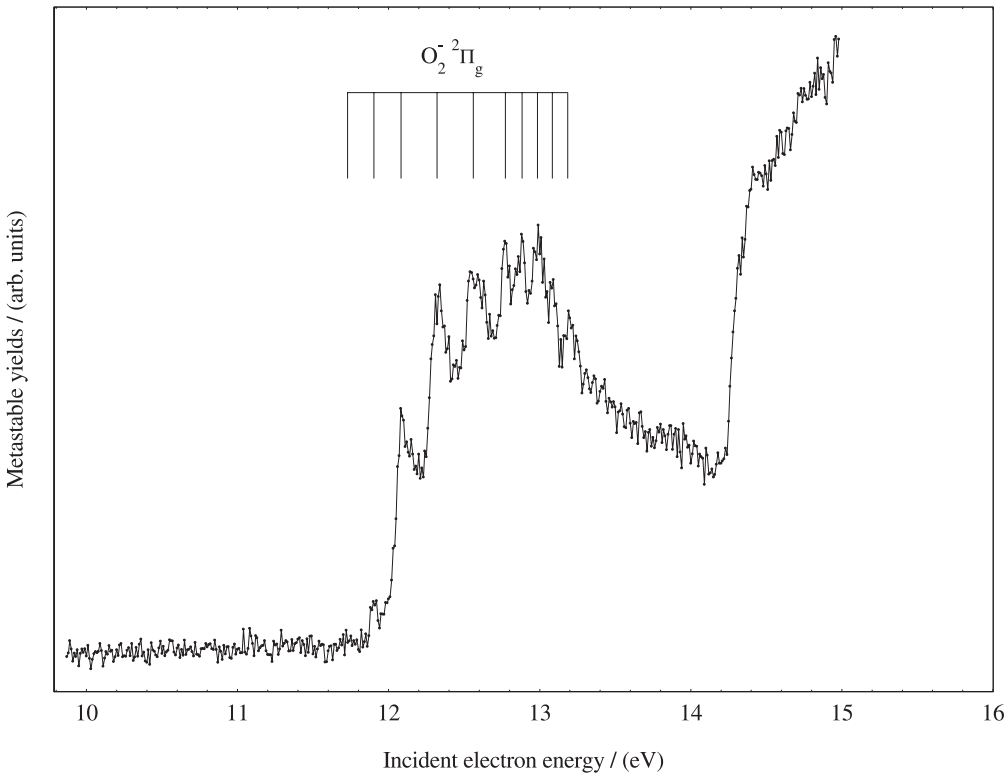

Fig. 3. The metastable excitation function of the O_2 spectrum showing O_2^- resonances in the energy region 10–15 eV.

Another series of resonances are obtained in a metastable excitation function spectrum shown in Figure 3. The figure shows an absence of the resonances in the first part of the spectrum up to 11.7 eV and groups of resonances in the energy region 11.7–13.2 eV, which is quite the opposite to the metastable spectrum of nitrogen [28] where resonances appeared in the part of the spectrum below the ionisation potential. The energy positions of the measured resonances are cited in Table 3. It is clear from the table that resonances don't have the same energy spacing. The first two resonances have a spacing of 0.17 eV, the next four resonances 0.24 eV and the last 5 resonances 0.1 eV indicating the existence of three different series. Concerning the energy spacing only the last 5 resonances can be compared with the series of resonances labelled as band "**a**" from Sanche and Schulz [10]. Unfortunately there is no good correlation in the energy positions between the two series except the last two resonances from band "**a**" ($\nu = 9$ and 10) whose excitation energies are close to the energies of the measured resonances at 12.77 and 12.88 eV respectively. Regarding the influence of the resonances on the intensity of the peaks in the threshold spectrum one can say that only two resonances at 11.73 and 11.90 eV have a relatively small influence on the intensity of $\nu' = 6$ and 7 of the $4^{1,3}\Pi_g$ Rydberg state. The metastable spectrum from Figure 3 shows a strong discontinuity and a sharp onset above 14.2 eV with a very strong rising continuum and above this energy shows no evidence for the existence of other resonances.

In the energy region 9.9–15.2 eV Sanche and Schulz [10] measured a large number of core excited resonances with the energies and their assignment cited in Tables 3 and 5. In the energy region above 11.8 eV they found two groups of resonances with a regular spacing assigned as band "**a**" and band "**b**" respectively.

3.7 Non-resonant scattering in the energy region 9.9–15.2 eV

In the energy region 9.9–15.2 eV the threshold electron impact spectrum shown in Figure 4 is characterized by an initial very strong feature followed by a number of lower intensity peaks continuing up to 15.2 eV. The identification of the features is made according to their energy positions, their energy spacings as well as from the comparison with the existing data from the literature.

3.7.1 Energy region 9.9–10.6 eV

The three features of different intensities at 9.970, 10.273 and 10.570 eV in the threshold spectrum occupy the energy region, which corresponds to the energy positions of the longest (LB), second (SB) and third band (TB) respectively. These three bands are well-known from the optical and energy loss measurements. Their classifications were the subject of many experimental and theoretical studies. It was not clear whether they belong to electronic states or vibrational levels of the same state. The confusion was the consequence of their unusual behaviour under different experimental conditions, which was the reason why

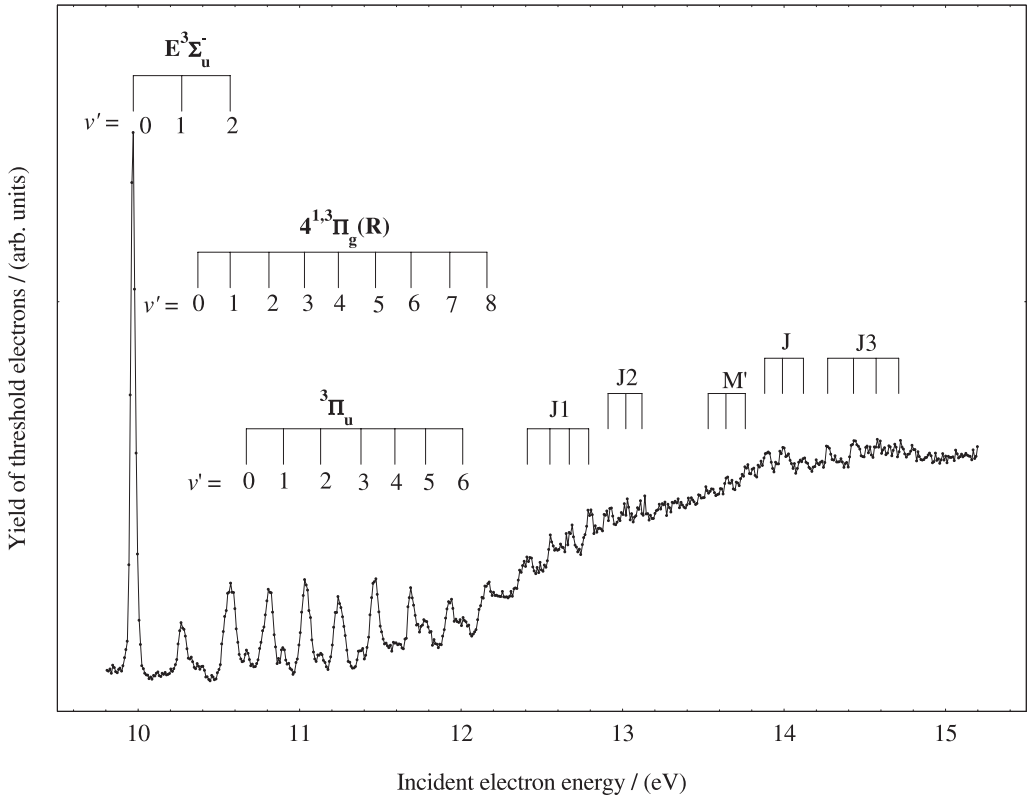

Fig. 4. Part of the threshold spectra from Figure 1 in the energy region 10–15.2 eV.

the energy loss measurements did not clarify that situation. On the other hand, in the theoretical calculations [29, 30] these three features are assigned as the vibrational levels of the $^3\Sigma_u^-$ state with energy positions different from the energy positions of the three bands. The computed energies are about 0.5 eV higher than those for the three bands but they have similar energy spacings. The calculated energy spacings are 0.37 and 0.33 eV, while the corresponding spacings of the three bands are 0.32 and 0.29 eV. In the identification of the first three features in the threshold spectrum in the energy region 9.9–10.6 eV, we accepted the argument of similar spacings and assigned them as the first three vibrational levels of the $E^3\Sigma_u^-$ state [31,32]. The energy positions of these features together with the result of York and Comer [22] are presented in Table 4. We note that the threshold spectra do not favorise the optically allowed transitions, which is the case for the $E^3\Sigma_u^-$ state but in this case resonant scattering is responsible for a strong enhancement of these features. According to Dillon et al. [33], the $E^3\Sigma_u^-$ state is composed of valence and Rydberg states of $^3\Sigma_u^-$ symmetry. The state is formed by the avoided crossing of the two potential curves, which represents the valence and Rydberg states of the same symmetry. The avoided crossing can explain the unusual behaviour of these three features under different experimental conditions due to a rapid change in the F-C envelope.

The $\nu' = 0$ of the $E^3\Sigma_u^-$ state in the threshold spectrum is the most prominent feature in the whole spectrum with a FWHM of 35 meV. As we explained earlier the intensity of the feature is the consequence of the resonant contribution (resonance **I**, [13]). The feature shows a symmetric profile, while in the energy loss experiment [22] it has an asymmetric shape with a long tail at the low-energy side and a sharp onset on the high-energy side. The $\nu' = 1$ of the $E^3\Sigma_u^-$ state presents an asymmetric feature with a much smaller intensity than the $\nu' = 0$ level. The shoulder on the high-energy side is due to the first level of the next $n = 4$ Rydberg series. The asymmetric shape of this feature was seen in the energy loss experiment [22] and in the photo absorption experiment [34] suggesting its complex nature. The $\nu' = 2$ level of the $E^3\Sigma_u^-$ state has an asymmetric profile and a higher intensity than the $\nu' = 1$ level. Its intensity can be the consequence of a resonant contribution.

The relative intensities of these three features in the threshold and energy loss spectra show a different form. The difference is in the intensity of the $\nu' = 1$ level. In the energy loss experiment this level is always higher than the $\nu' = 2$ level, what is the opposite to the threshold spectrum.

3.7.2 Energy region 10.3–12.2 eV-Rydberg states

This energy region in the threshold spectrum is shown in Figure 4. The classification of the measured features in this energy region was not obvious despite the simplicity of the spectrum, which shows only two regularly spaced vibrational series present in the form of doublet peaks with

different intensities. Unfortunately, there are no other threshold spectra with which to make a comparison as well as precise theoretical calculations. There are only two experiments for comparison, one is the energy loss experiment with high precision and low impact energy [22] and the other is from REMPI spectroscopy [35]. From the theoretical side only calculations [1,29] are any value. The excitation energies of the measured features from the present experiment together with the results [22,35] are summarised in Table 4 which shows a good agreement in the excitation energies of the measured features in the three experiments.

The $4^{1,3}\Pi_g$ Rydberg state

Following the potential energy diagram for the O_2 molecule [1] and a good agreement in the energy positions between our results and [35], regularly spaced intense features with a FWHM between 50 and 60 meV are assigned to the $4^{1,3}\Pi_g$ Rydberg state. Due to a poor energy resolution of the spectrometer the threshold spectrum does not show the differences between the singlet and triplet states (25 meV). In REMPI spectroscopy [35] five vibrational levels of the $n = 4\ ^3\Pi_g$ Rydberg and four vibrational levels of the $n = 4\ ^1\Pi_g$ Rydberg state were measured, while the present measurement shows 9 vibrational levels. Table 4 shows an excellent agreement in the energy positions of the vibrational levels in the two experiments. In contrast, York and Comer [22] did not classify the measured features found in the energy loss experiment concerning this energy region. One must note the excellent agreement in energy positions between the measured features in the present experiment and those by York and Comer [22]. These features had been measured earlier [34,36–38].

The $\nu' = 0$ of the $4^{1,3}\Pi_g$ Rydberg state at an energy of 10.367 eV is present in the form of the shoulder with a low intensity probably due to a weak coupling between the ground state of the O_2 molecule and the $n = 4$ Rydberg state in the F-C region which is clearly shown in the potential energy diagram for O_2 [1]. The weak coupling is the consequence of different equilibrium nuclear positions between the Rydberg and ground state of O_2 in the F-C region. The diagram also shows the perturbation of the Rydberg state by the $II^1\Pi_g$ valence state. The $\nu' = 1$ of the $4^{1,3}\Pi_g$ Rydberg state coincides in energy position with the $\nu' = 2$ of the $E^3\Sigma_u^-$ state and probably contributes to the intensity of this level. The remaining levels of the $n = 4$ Rydberg state are present in the form of peaks with similar intensities but they are not enough separated from the accompanying $^3\Pi_u$ series.

The $^3\Pi_u$ state

Another state in the threshold spectrum present in the form of 7 vibrational levels equally spaced with smaller intensities than the accompanying $n = 4$ Rydberg series is tentatively assigned as the $^3\Pi_u$ Rydberg state. The assignment is made according to theoretical calculations [29] which shows the potential energy curve for this state with energy of 10.75 eV, and that is close to the energy position of $\nu' = 0$ in the measured series (10.672 eV). In the absence of other theoretical calculations and similar experiments to confirm this assignment, we accepted the suggestion from [29]. The only energy loss data for comparison are those from York and Comer [22]. The measured features in their experiment do not show any regularity in intensities and the authors left them without classification. For the feature at 10.664 eV they found a rapid change in intensity with scattering angle suggesting that it could be due to a transition forbidden by both spin and symmetry selection rules.

Table 4 shows the energy positions of the $^3\Pi_u$ state together with the results [22]. It is clear that a good agreement between the two measurements exists in the energy positions of the measured features. These features were measured earlier [34,36,38].

3.7.3 Energy region above the first ionisation potential

The first ionisation potential of $O_2(X^2\Pi_g)$ at 12.07 eV [39] is present in the form of a minimum similar to the threshold spectrum of CO [40]. The feature does not show the shape of the ionisation cusp that was measured in helium [6] due to Rydberg series converging to higher ionisation potentials. The features above the ionisation potential are present in the form of peaks with small intensities. The underlying continuum arises from zero energy electrons from the ionisation process of the O_2 molecule. This energy region of O_2 has been studied extensively both in photo absorption and energy loss experiments at high impact energy and small angle. Both measurements confirm the existence of strong bands known through the literature as Hopfield bands. They were grouped into vibrational series [41] as an electric dipole allowed transition. This was confirmed in the energy loss experiments [38,42–44]. Katayama and Tanaka [45] have revised the assignment of these progressions suggesting the existence of two Rydberg progressions, which converge to the second ionisation potential $a^4\Pi_u$ at 16.101 eV. However at low impact electron energy the spectrum shows fewer features with low intensities as was seen in the energy loss experiment [22] (10 eV, 90°). The characteristic of the threshold spectrum in the energy region 12.2–5.2 eV is the existence of 5 separate groups superimposed on the rising continuum. The identification of the observed features was not so obvious. Only two groups **M'** and **J** have energy positions which coincide with energy positions of the vibrational levels of the Hopfield bands. Three other groups are assigned as **J1**–**J3** similar to those in the energy loss experiment of York and Comer [22] who labelled the features as groups (**i**)–(**v**). According to the vibrational constants and energy locations they suggest that the measured features are associated with the spin forbidden counterparts of the bands **H**, **H'**, **M** and **M'**. The excitation energies of the features are given in Table 5 together with the present results. The table shows an excellent agreement in the energy positions in the two experiments.

The first four features labelled **J1** are positioned in the region of band **H**. The energy difference between the corresponding vibrational levels in the two series is 70 meV.

In this energy region Sanche and Schulz [10] measured 6 vibrational levels of a resonance labelled as band "**a**". The threshold spectrum shows that these resonances have no influence on the intensity of the measured features. The next series of three peaks labelled **J2** partly occupy the energy region of band **H'**. Again as in the previous case the agreement in the energy positions between the measured features and those of York and Comer [22] labelled (**ii**) is excellent. According to their energy positions the next series of 6 peaks are identified as members of two bands **M'** and **J**. These bands belong to the optically allowed transitions and hence they are present in the threshold spectrum with low intensities. The last group of three peaks labelled **J3** has a good agreement in energy position with series (**iii**) of York and Comer [22]. According to [22] these peaks belong to the symmetry forbidden transitions. The series **J3** occupy the same energy region as the group of 4 resonances known as band "**b**" [10], but the intensity of the peaks are not influenced by these resonances.

4 Conclusion

In this measurement we used a high resolution electron spectrometer with an incident beam and a threshold analyser with a high sensitivity for zero energy electrons which enables us to study processes very close to the threshold energies of the excited states of the O_2 molecule. The large number of features which correspond to optically forbidden states and core excited resonances were observed and identified according to their energy positions and energy spacings between vibrational levels. A good agreement was achieved in the energy positions between the measured features and corresponding data in the literature.

We wish to acknowledge to Dr. V. Bocvarski and Dr. V. Cvjetkovic for their participation in the data treatment, and Dr. B. Marinkovic for his critical reading of the paper. This work was partly supported by RZN- Serbia.

References

1. J.S. Morrill, M.L. Ginter, B.R. Lewis, S.T. Gibson, J. Chem. Phys. **111**, 173 (1999)
2. P.H. Krupenie, J. Phys. Chem. Ref. Data **1**, 423 (1972)
3. B.L.G. Bakker, D.H. Parker, J. Chem. Phys. **112**, 4037 (2000)
4. M. Allan, J. Phys. B: At. Mol. Opt. Phys. **28**, 4329 (1995)
5. S. Cvejanovic, J. Jureta, M. Minic, D. Cvejanovic, J. Phys. B: At. Mol. Opt. Phys. **25**, 4337 (1992)
6. S. Cvejanovic, F.H. Read, J. Phys. B: At. Mol. Phys. **7**, 1180 (1974)
7. S. Cvejanovic, J. Jureta, D. Cvejanovic, J. Phys. B: At. Mol. Phys. **18**, 2541 (1985)
8. C.J. Noble, P.G. Burke, J. Phys. B: At. Mol. Phys. **19**, L35-L39 (1986)
9. D. Teillet-Billy, L. Malegat, J.P. Gayacq, J. Phys. B: At. Mol. Opt. Phys. **20**, 3201 (1987)
10. L. Sanche, G.J. Schulz, Phys. Rev. A **6**, 69 (1972)
11. J. Jureta, S. Cvejanovic, unpublished
12. D. Spence, J. Chem. Phys. **74**, 3898 (1981)
13. J. Jureta, S. Cvejanovic, D. Cvejanovic, V. Bocvarski, V. Cvjetkovic, in *Proceedings of the XXI ICPEAC*, Santa Fe, USA 2001, edited by S. Datz, M.E. Bannister, H.F. Krause, L.H. Saddiq, D. Schulz, C.R. Vane, p. 235
14. D.C. Cartwright, N.A. Fiamengo, W. Williams, S. Trajmar, J. Phys. B: At. Mol. Phys. **9**, L419 (1976)
15. L.C. Lee, T.G. Slanger, G. Black, R.L. Sharpless, J. Chem. Phys. **67**, 5602 (1977)
16. R.J. Buenker, S.D. Peyerimhoff, M. Peric, Chem. Phys. Lett. **42**, 383 (1976)
17. P.S. Julienne, D. Neumann, M. Krauss, J. Chem. Phys. **64**, 2990 (1976)
18. R.P. Saxon, B. Liu, J. Chem. Phys. **67**, 5432 (1977)
19. D.C. Cartwright, W.J. Hunt, W. Williams, S. Trajmar, W.A. Goddard, Phys. Rev. A **8**
20. S. Trajmar, D.C. Cartwright, R.I. Hall, J. Chem. Phys. **65**, 5275 (1976)
21. R.H. Huebner, R.J. Celotta, S.R. Mielczarek, C.E. Kuyatt, J. Chem. Phys. **63**, 241 (1975)
22. T.A. York, J. Comer, J. Phys. B: At. Mol. Phys. **16**, 3627 (1983)
23. A. Sur, C.V. Ramana, S.D. Colson, J. Chem. Phys. **83**, 904 (1985)
24. W.J. van der Zande, W. Koot, J. Los, J.R. Peterson, J. Chem. Phys. **89**, 6758 (1988)
25. R.P. Saxon, B. Liu, J. Chem. Phys. **73**, 870 (1980)
26. A. Sur, R.S. Friedman, P.J. Miller, J. Chem. Phys. **94**, 1705 (1991)
27. Y. Li, I.D. Petsalakis, H.P. Libermann, G. Hirsch, R.J. Buenker, J. Chem. Phys. **106**, 1123 (1997)
28. P. Hammond, G.C. King, J. Jureta, F.H. Read, J. Phys. B: At. Mol. Phys. **20**, 4255 (1987)
29. R.J. Buenker, S.D. Peyerimhoff, Chem. Phys. Lett. **34**, 225 (1975)
30. M. Yoshimine, K. Tanaka, H. Tatewaki, S. Obari, E. Sasaki, K. Onno, J. Chem. Phys. **64**, 2254 (1976)
31. B.R. Lewis, J.P. England, S.T. Gibson, M.J. Brunger, M. Allan, in *Proceedings of the, XX ICPEAC*, Vienna, Austria 1997, edited by F. Aumayer, G. Betz, H.P. Winter, p. 087
32. W.F. Chan, G. Cooper, C.E. Brion, Chem. Phys. **170**, 99 (1993)
33. M. Dillon, M. Kimura, R.J. Buenker, G. Hirsch, Y. Li, L. Chantranupong, J. Chem. Phys. **102**, 1561 (1995)
34. Y. Tanaka, J. Chem. Phys. **20**, 1728 (1952)
35. R.J. Yokelson, R.J. Lipert, W.A. Chupka, J. Chem. Phys. **97**, 6153 (1992)
36. R.E. Huffman, J.C. Larabee, Y. Tanaka, J. Chem. Phys. **40**, 356 (1964)
37. R.J. Collins, D. Husain, R.J. Donovan, J. Chem. Soc. Faraday Trans. II **69**, 145 (1973)
38. J. Geiger, B. Schröder, J. Chem, Phys. **49**, 740 (1968)
39. K.P. Huber, G. Hezrzberg, *Molecular spectra and molecular structure IV, Constans of Diatomic Molecules* (Van Nostrand, New York, 1979)
40. P. Hammond, G.C. King, J. Jureta, F.H. Read, J. Phys. B: At. Mol. Phys. **18**, 2057 (1985)
41. W.C. Price, G. Collins, Phys. Rev. **48**, 714 (1935)
42. E.N. Lassettre, A. Skerbele, M.A. Dillon, K.J. Ross, J. Chem. Phys. **48**, 5066 (1968)
43. R.H. Huebner, R.J. Celotta, S.R. Mielczarek, C.E. Kuyatt, J. Chem. Phys. **63**, 241 (1975)
44. E. Lindholm, Ark. Fys. **40**, 117 (1969)
45. D.H. Katayama, Y. Tanaka, J. Mol. Spectrosc. **88**, 41 (1981)